Ecological Engineering 180 (2022) 106678

Contents lists available at ScienceDirect

Ecological Engineering

journal homepage: www.elsevier.com/locate/ecoleng

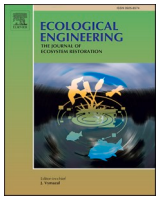

Variation of mean flow and turbulence characteristics within canopies of restored intertidal oyster reefs as a function of restoration age

David Cannon [a,*], Kelly M. Kibler [a], Vasileios Kitsikoudis [b], Stephen C. Medeiros [c], Linda J. Walters [d]

[a] Department of Civil, Environmental, and Construction Engineering and National Center for Integrated Coastal Research, University of Central Florida, Orlando, FL 32816, USA
[b] Water Engineering and Management, Faculty of Engineering Technology, University of Twente, Enschede, the Netherlands
[c] Department of Civil Engineering, Embry-Riddle Aeronautical University, Daytona Beach, FL 32114, USA
[d] Department of Biology and National Center for Integrated Coastal Research, University of Central Florida, Orlando, FL 32816, USA

ARTICLE INFO

Keywords:
Boundary layer
Crassostrea virginica
Oyster reef
Restoration
Turbulence

ABSTRACT

The ecological benefits of healthy oyster populations have led to mounting interest in restoration of degraded reef habitats and design of nature-based reef features. However, hydrodynamic studies of restored oyster reef remain sparse, and little is known about changes in mean flow and turbulence as a function of time since restoration. In this study, we investigate hydrodynamic differences between restored (restoration age: <1 y, 2 y, 4 y), degraded, and intact intertidal oyster reefs in a shallow, microtidal estuary. Field experiments conducted at each reef were designed to characterize variability in flow and turbulence associated with differences in reef morphology and restoration age, addressing research questions of whether and when hydrodynamic function is reestablished following restoration. Minor differences in normalized turbulence parameters within the canopies of restored and reference reefs (2 cm above bottom) were associated with variable channel-to-reef velocity attenuation, which was linked to heterogeneity in oyster canopy structure as characterized by high-resolution laser scans. Within-canopy turbulence characteristics and normalized Reynolds stresses were significantly elevated on restored and reference reefs compared to the degraded reef, emphasizing the role of reef restoration in changing near-bed hydrodynamics. Above-canopy (9 cmab) turbulence was hydrodynamically similar across live reference and restored reefs of all restoration ages, with estimated roughness heights that scaled with the canopy height. Comparisons between intact and restored reefs indicate that properly restored reefs can reach hydrodynamic similarity with historically intact reefs within 1 year of restoration, a conclusion that supports the use of reef restoration as a tool to reestablish hydrodynamic functions on degraded reefs.

1. Introduction

Oysters are ecologically and economically important components of shallow coastal ecosystems (Grabowski et al., 2012). Oyster reefs provide habitat to support diverse species assemblages (Coen et al., 1999), improve water quality (Dame et al., 1989), sequester carbon (Fodrie et al., 2017; Veenstra et al., 2021), stabilize coastal habitat (Meyer et al., 1997; McClenachan et al., 2020), and increase landscape diversity (Coen and Luckenbach, 2000). Over the last century, oyster populations have decreased by an estimated 85% globally (Beck et al., 2011), and many traditionally reef-based ecosystems are nearly devoid of oysters in the present day (Chesapeake Bay: Schulte et al., 2009, Wilberg et al., 2011; Hudson-Raritan Estuary: McFarland and Hare, 2018; Australia: Gillies et al., 2017, Ogburn et al., 2007). As such, coastal management agencies have placed renewed value on healthy oyster populations, with restoration initiatives aimed at restoring lost ecosystem services and improving resilience to exogenous environmental changes, including sea level rise (Rodriguez et al., 2014; Solomon et al., 2014).

As reef-building "ecosystem engineers," oysters actively change the environment they inhabit, inducing dramatic changes in both the local flow field (Lenihan, 1999; Reidenbach et al., 2013) and the chemical properties of the water column and reef sediments (Chambers et al.,

* Corresponding author at: Cooperative Institute for Great Lakes Research (CIGLR), School for Environment and Sustainability (SEAS), University of Michigan, Ann Arbor, MI 48109, USA.
E-mail address: djcannon@umich.edu (D. Cannon).

https://doi.org/10.1016/j.ecoleng.2022.106678
Received 9 March 2022; Received in revised form 22 April 2022; Accepted 1 May 2022
Available online 6 May 2022

2018; Locher et al., 2020). Oyster reefs are complex in terms of both structure and function. At the largest scale, the bulk reef structure creates a heterogeneous bedform with potential to direct local flows, influence mixing, and alter the chemical composition of water (Kaplan et al., 2016). On the surface of natural reefs, oysters form vertically-oriented clusters that protrude above the reef bed into the water column, creating a roughness sublayer that is several orders of magnitude larger than the roughness height of mud and sand substrates (Stiner and Walters, 2008; Styles, 2015). These heterogeneous three-dimensional oyster canopies alter local and regional hydrodynamics through roughness enhancement (Styles, 2015), bed alteration (Colden et al., 2016), and active filtration (Porter et al., 2004), which in turn affects nutrient cycling and sediment transport among other processes (e.g. Gutiérrez et al., 2003). This roughness layer can be considered a canopy-like structure, similar to canopies of other benthic organisms (i.e. submerged vegetation: Nepf, 2012, corals: Davis et al., 2021). Most hydrodynamic field studies in the vicinity of oyster reef have focused on characterizing roughness effects above the canopy (e.g. Lenihan, 1999; Reidenbach et al., 2013; Whitman and Reidenbach, 2012; Styles, 2015), but within-canopy hydrodynamics are salient to functions of larval recruitment and settling (Whitman and Reidenbach, 2012; Hubbard and Reidenbach, 2015), flow attenuation (Cannon et al., 2022), and benthic fluxes (Kitsikoudis et al., 2020; Reidenbach et al., 2013). As such, better understanding of flow dynamics within and above oyster canopies has application to reef restoration, management of natural reefs, and design of functional nature-based features that fulfill both ecological and engineering goals.

Although restoration or ecological engineering as applied to nature-based design are undertaken with intention to recover lost ecosystem services (e.g. Elliott et al., 2016), it is unclear how quickly these services emerge after new oyster reefs are constructed or degraded reefs are restored (Elliott et al., 2007). The time scales of recovery are expected to vary based on the service of interest (Peterson et al., 2003; Barber et al., 2010; La Peyre et al., 2014), with some ecosystem services returning as soon as live oyster clusters and three-dimensional structures are present (e.g. habitat provision, local hydrodynamic influence, shoreline stabilization), and others occurring over longer timescales (i.e. years to decades) as the reef matures and becomes self-sustaining (e.g. water quality enhancement, oyster harvesting, landscape-scale flow control). While previous studies have largely focused on the temporal development of higher order ecosystem services on restored reefs (e.g. La Peyre et al., 2014; Walles et al., 2016), more fundamental questions on the evolution of reef hydrodynamics (i.e. wave or current attenuation, turbulence characteristics) with restoration age remain unaddressed. Understanding these fundamental changes in the flow field and how they evolve with time since restoration is an important component of restoration initiatives, especially considering the direct link between hydrodynamic alterations and desired restoration outcomes.

The objective of this study is to understand how hydrodynamics within and above the canopy of restored intertidal oyster reef vary with time after restoration. The primary research question addressed is whether hydrodynamic functions within restored oyster reef of various restoration age (6 months, 2 years, 4 years) are similar to those within natural, reference-condition reef. Hydrodynamic measurements were collected in the field both within and above the canopies of *C. virginica* (Eastern oyster) reefs to examine variations in turbulence and flow attenuation in both flow regions, and 3D laser scans were used to provide detailed canopy structure characterizations at each reef. This is one of very few studies to examine the coupled structural and hydrodynamic differences between natural and restored intertidal oyster reefs, and it is the first to investigate drivers of hydrodynamic change over time after restoration. Investigation within the oyster canopy offers particularly novel insights with application not only to reef restoration strategies, but to design of nature-based features.

2. Methodology

2.1. Study area

Field experiments were conducted in Mosquito Lagoon, a shallow (mean depth: 1.5 m) microtidal estuary along the Atlantic coast of Florida, USA (Fig. 1). The 85 km^2 waterbody is connected to the marine system at the northern end through the narrow (400 m) Ponce de Leon Inlet. Climatic conditions of Mosquito Lagoon are humid subtropical (temperature: 25–30 °C; salinity: 10–40 ppt; Down and Withrow, 1978) and water levels vary seasonally and semidiurnally with tides (tidal range in study sites: ±20 cm). Proximity to Ponce de Leon Inlet defines physical habitat conditions throughout the lagoon. The northern portion of the lagoon is a complex of channels flowing through a maze of sandy shoals and quasi-stable mangrove and salt marsh wetlands established upon the tidal delta (Mehta and Brooks, 1973). Eastern oysters are abundant in the northern reach of the water body (Garvis et al., 2015), where tidal influences are strongest. Here, intertidal reef is a prevalent landscape feature, occupying margins of mangrove wetlands and forming extensive complexes within shallow, protected shoals between vegetated islands.

Hydrodynamic measurements and laser scans were collected from five intertidal oyster reefs in northern Mosquito Lagoon (Fig. 1, Table 1): three restored reefs, where field observations occurred within a year (R-2017), two years (R-2016), and four years (R-2014) after the time of restoration, one reference-condition intact oyster reef (Reference), and one degraded reef with no live oysters (Degraded) which was similar to the condition of restored reefs before restoration. The restored and degraded reefs investigated in this study were historically colonized by oysters, and previous data collection suggest that reef degradation was the result of anthropogenic pressures (i.e. recreational boat wakes) and not changes to site chemistry (e.g. pollution, acidification, etc.) or disease (Grizzle et al., 2002; Walters et al., 2007; Stiner and Walters, 2008; Garvis et al., 2015). The restored reefs were all restored using identical oyster mat materials and techniques, described in detail in Garvis et al. (2015). Reef crest elevations were initially lowered to low intertidal height relative to nearby intact reefs, and oyster mats made of Vexar™ extruded polyethylene mesh were deployed across the reef surface and held down with concrete irrigation weights. Importantly, each oyster mat was constructed with 36 attached adult *C. virginica* shells oriented in the vertical position in order to mimic the structure of reference reefs and promote natural oyster recruitment at the restoration sites. Oysters were allowed to recruit naturally without larvae seeding. Reefs were chosen for this study to represent a developmental continuum between pre-restoration (Degraded) and fully intact (Reference) reef structure. From the available population of reefs, study reefs were chosen such that fetch, adjacent channel depths and channel flow velocities were similar across all sample locations.

2.2. Field observations

Hydrodynamic measurements were collected from within and directly above oyster reef canopies during low and high seasonal water levels, respectively, in order to compare mean flow and turbulence between reefs in different canopy positions. No simultaneous measurements were collected both above and within the oyster canopy. Current velocities were measured concurrently within or above the reef canopy and offshore in the main channel (10–15 m from reef crest). Reef velocity profiles (resolution: 1 mm resolution) were sampled at 100 Hz using a Nortek Vectrino Profiler, positioned such that the non-biased portion of the profile fell between 1.5 and 2.5 cm above the bed for within-canopy measurements and 9–10 cm above the bed for above-canopy measurements. This placed the most accurate portion of the profiles (5 cm below the probe; Thomas et al., 2017), at approximately 2 cm and 9.5 cm above the bed, respectively. Above-canopy measurements were not collected over the degraded reef, which lacked canopy.

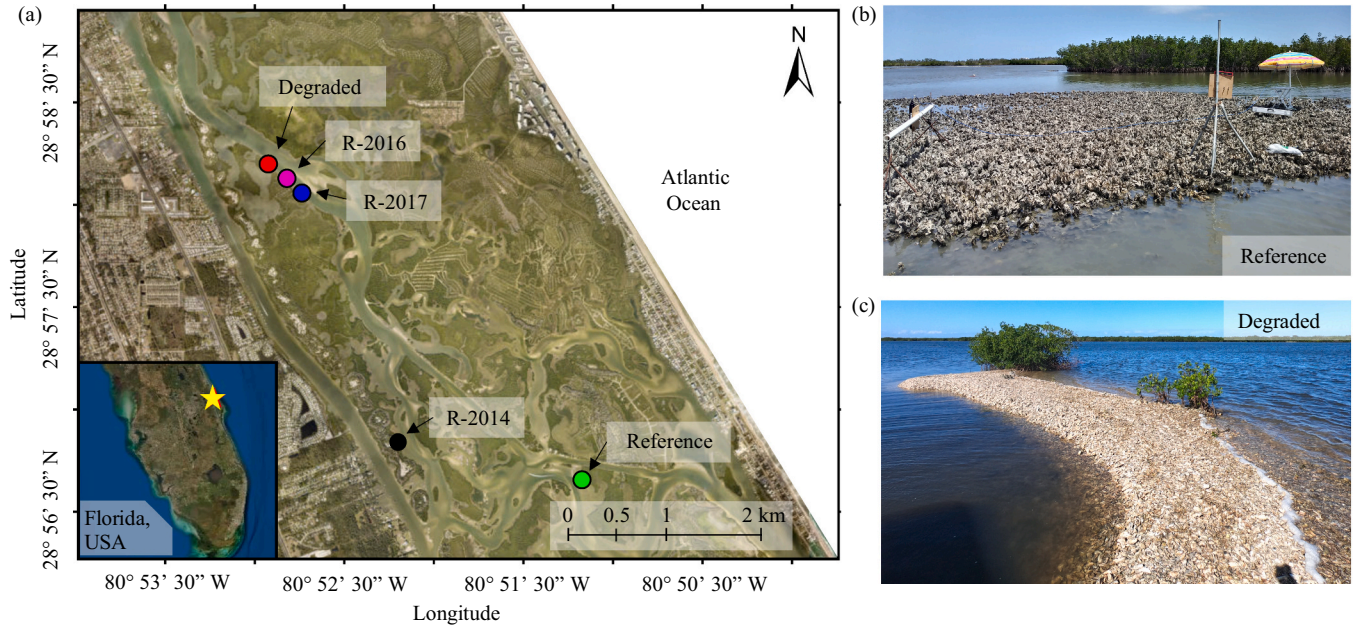

Fig. 1. (a) Map of study area, including the five study reefs (colored circles: Degraded, R-2017, R-2016, R-2014, and Reference) and location along the coast of Florida, USA (inset diagram). Representative photos of oyster structure on the (b) reference and (c) degraded reefs are included for reference.

Table 1
Oyster reef characteristics for each sample location: live oyster density, canopy element density, reef slope (mean [max]), canopy height, solid volume fraction, mean organic matter content (OM) of reef and {channel} sediments, and reef sediment grain sizes D_{50} and (D_{84}). Solid volume fractions are reported both reef-wide (mean ± 95% confidence interval) and locally in the vicinity of the reef velocity probe [mean]. Due to lack of canopy on the degraded reef (*), surface roughness is reported as the D_{50} of surface particles (i.e. median particle size).

Reef name	Live oyster density oysters/m^2	Canopy element density el./m^2	Canopy Height: h_s cm	Reef slope m/m	Solid volume fraction: SVF %	OM content %	Sediment grain size: D_{50} (D_{84}) mm
Reference	184 ± 34	168	6.0 ± 0.1 [8.2]	0.06 [0.50]	7.6 ± 0.2 [6.1]	8.3 {1.5}	1.2 (21)
R-2017	250 ± 13	84	5.6 ± 0.3 [5.9]	0.08 [0.20]	7.6 ± 0.3 [10.6]	11.9 {2.1}	2.2 (19)
R-2016	208 ± 7	96	5.5 ± 0.2 [7.6]	0.09 [0.19]	7.5 ± 0.3 [10.2]	9.0 {1.7}	1.3 (18)
R-2014	475 ± 41	88	8.3 ± 0.2 [5.2]	0.18 [0.49]	10.7 ± 0.3 [11.8]	12.1 {2.8}	5.8 (20)
Degraded	0	N/A	1.0 ± 0.2*	0.13 [0.28]	N/A	7.8 {3.5}	0.98 (17)

Offshore channel velocities were measured within at least 50 cm of the bed (2 cm resolution) using a 2 MHz Nortek Aquadopp HR Profiler (sample rate: 2 Hz). The instrument was deployed in down-looking orientation near the water surface. The channel bottom was identified using instrument-measured signal amplitude profiles (e.g. Kitsikoudis et al., 2020), and measurement cells within 5 cm of the bed were removed due to acoustic backscatter. All velocimeters were aligned to a common coordinate system, such that $\overline{u}$, $\overline{v}$, and $\overline{w}$ represent streamwise (reef-parallel), cross-shore, and vertical velocity components, respectively. All velocity measurements were collected continuously for 2–4 h during the flood tide, where the flow speed was approximately steady.

Local forcing conditions, including wind speeds and direction, wave heights, and water depths, were measured continuously over each deployment. Wind speeds and directions were recorded approximately 2 m above the water surface (60 s interval) using a Davis Wind Speed and Direction Smart Sensor (Onset, S-WCF-M003) deployed in the channel. Depth was measured with a pressure logger (Onset U20L-04) deployed near the Aquadopp HR Profiler. Sonic water surface loggers (Ocean Sensor Systems XB Pro) were deployed near each velocimeter to characterize on-reef and off-reef (i.e. channel) surface waves. The continuous 32 Hz water surface deformation time series was used to calculate significant wave height ($H_s = 4\sigma_s$) over 2 min (50% overlap) data segments (Dean and Dalrymple, 1991).

High resolution three-dimensional oyster canopy measurements were captured in detail using a laser scanner (Faro x330), which was deployed at low tide when the reef surface was fully exposed. At each reef, the laser-scanner was repositioned several times to capture roughness elements at multiple angles, minimizing the effects of "shadows" in the final laser scan point cloud. Bulk reef slope and channel bathymetry were measured using a CHC X91+ real time kinematic (RTK) GNSS surveyor. Point measurements were collected within the oyster canopy on the true reef bed (i.e. below the canopy roughness elements) using a topo shoe. Elevations are reported in reference to NAVD-88 (2011) using GEOID12A. Referencing elevations to mean sea level was inhibited by a lack of local reference data and poorly parameterized tidal transformations in the study area (e.g. White et al., 2016). Reef canopy height was also characterized manually during low water levels. Within a 0.25 m^2 quadrat centered around the Vectrino location, every solid element (either individual oysters or clusters of oysters) was measured with calipers along the vertical and largest horizontal axes. Live oyster density was measured during low water levels by counting all live *C. virginica* in 30 haphazardly placed 0.25 m^2 quadrats on each reef surface. Laser scans, local roughness estimations, and live oyster counts were accomplished within the same month. Although reef morphology may evolve over time, we assume that the bulk roughness parameters assessed for each reef remained consistent over the course of data collection for this study (~6 months). No extreme hydrodynamic events (e.g. hurricanes) or mass oyster mortalities occurred during the study period.

Sediment characteristics were assessed at each reef using bulk

sediment cores collected on the reef surface and in the adjacent channel. Five replicate cores (diameter: 7.2 cm) from the reef and five cores from the channel of each site were extracted to a sediment depth of approximately 15 cm and water trapped in the coring tube was retained. Sediment samples were oven dried at 110 °C for more than 24 h and particles were carefully manually separated. Organic matter content (OM) was evaluated for each core from the mass lost on ignition (16 h at 550 °C) of 20 g samples of sand and finer sediments (D < 2 mm). Replicate cores from each site and location (reef and channel) were pooled for particle size analysis, assessed using a combination of wet and dry sieve analysis to improve the accuracy of mass estimates for silt and clay sediments (ASTM, 2006, 2013).

2.3. Data analysis

2.3.1. Laser scan analysis

The canopy heights and solid volume fractions (SVFs) for reference and restored reef canopies were computed from high-resolution topographic laser scans. Reef scans were subdivided into 0.5 × 0.5 m computation grids and a sloped ordinary least squares (OLS) regression plane was fit to the lowest points in each grid to approximate the local bed slope. 2500 points were then randomly selected in each grid to account for variable point densities, resulting in an average density of 1 point/cm^2. Grids with fewer than 2500 points were removed, as were all grid cells containing water or vegetation. The canopy height associated with each cell was estimated as the average height of all points above the regression plane, while the solid volume was computed by integrating the area between the heterogeneous reef surface and the regression plane. The total solid volume fraction (SVF) was then calculated using a reference volume of 0.125 m^3, which corresponds to a local depth of 25 cm (i.e. the largest observed canopy height). Choosing a consistent depth across sites to compute sample volume allows for direct comparisons of solid volume fraction between study reefs.

2.3.2. Hydrodynamic analysis

Velocity time series were quality controlled by removing measurements with poor signal-to-noise ratios (SNR < 20) and low correlations (< 80%), and resulting gaps in the data series were replaced via linear interpolation. Data affected by the wakes of passing boats were removed. Each time series was despiked using a phase-space thresholding algorithm (Goring and Nikora, 2002; Wahl, 2003). Mean velocity profiles were computed using quality-controlled time series averaged over 120 s of sampling (50% overlap). For all analyses, we assume that the flow is steady over each 2 min data segment. Depth-integrated streamwise and cross-shore channel velocities ($\overline{u_{CH}}$, $\overline{v_{CH}}$) were calculated using offshore velocity profiles measured within 50 cm of the bed. Mean channel-to-reef velocity attenuation was calculated from depth-integrated channel velocities and reef velocities taken from the profile midpoint, with attenuation (A_S) defined as the best-fit slope of the linear model defined by $\overline{U_R} = (1 - A_S) \bullet \overline{U_{CH}} + b$ where $\overline{U_{CH}} = \left(\overline{u_{CH}}^2 + \overline{v_{CH}}^2\right)^{1/2}$ and $\overline{U_R} = \left(\overline{u_R}^2 + \overline{v_R}^2\right)^{1/2}$ are horizontal flow speeds measured in the channel and above the reef, respectively, and b is the intercept of the best-fit attenuation slope.

Quality-controlled turbulent time series collected within/above the reef canopy with the Vectrino Profiler were used to calculate wave-removed estimates of the Reynolds stress tensor. Although observed wave heights were small (max H_s<10 cm, typically <5 cm), the weakly energetic current (U_{reef} < 25 cm/s) and shallow water depths (10–30 cm) above each reef led to outsized energy contributions from even low magnitude surface gravity waves. Instantaneous velocity measurements (u_i) were the result of wave oscillations ($\tilde{u}_i$), turbulent fluctuations (u_i'), and mean flow ($\overline{u_i}$), such that

$$u_i = \overline{u}_i + \tilde{u}_i + u_i'$$

where u_i represents the three-dimensional velocity vector (u,v,w). For each 120 s data segment, velocity measurements were linearly detrended to remove the energy associated with the mean flow ($\overline{u_i}$), and fluctuations associated with surface waves ($\tilde{u}_i$) and turbulence (u_i') were separated using the phase method (Bricker and Monismith, 2007). After estimating the power spectral density for a single velocity component (u, v, or w), the energy contributions due to waves ($\overline{\tilde{u}_i^2}$) and turbulence ($\overline{u_i'^2}$) were separated using a best-fit line interpolated across the surface-wave frequency band, visually identified as 0.3 < f < 2 Hz. Energy associated with waves and turbulence were then decoupled and used to calculate wave-removed estimates of the Reynolds stress tensor following the methods described in Bricker and Monismith (2007). As discussed in previous studies (e.g. Hansen and Reidenbach, 2017), squared horizontal turbulent velocity fluctuations (i.e. $\overline{u_i'^2}$) are prone to large errors when estimated using the phase method, especially when wave energy contributions are large (e.g. Hansen and Reidenbach, 2017). As such, we limit our analysis to the cross-correlation terms ($\overline{u'w'}$, $\overline{v'w'}$) and the turbulent energy of the vertical velocity ($\overline{w'^2}$), which was only marginally affected by waves due to the elliptical structure of the wave-induced orbital velocities (i.e. shallow-intermediate waves). All data segments with wave energy contributions greater than 50% ($\frac{\overline{\tilde{w}^2}}{\left[\overline{w'^2}+\overline{\tilde{w}^2}\right]} > 0.5$) were removed from analysis to minimize bias induced by phase decomposition. This ensures that the majority of fluctuation energy contained in each burst is related to turbulence rather than waves. Turbulence estimates were further refined by removing Doppler noise, which was identified and removed following the methods outlined in Thomas et al. (2017), developed explicitly for use with the Nortek Vectrino Profiler. Importantly, all discussion of turbulence characteristics will be limited to measurements collected around the sample profile midpoint, where Doppler noise is weakest (Thomas et al., 2017).

After phase decomposition and noise removal, finalized turbulence estimates were used to calculate the total Reynolds shear stress $\left(\tau_{RS} = \rho\sqrt{\overline{u'w'}^2 + \overline{v'w'}^2}\right)$ and turbulent production $\left(P = -\overline{u'w'}\frac{\partial \overline{u}}{\partial z} - \overline{v'w'}\frac{\partial \overline{v}}{\partial z}\right)$, where $\frac{\partial \overline{u}}{\partial z}$ and $\frac{\partial \overline{v}}{\partial z}$ are the velocity gradients estimated from averaged velocity profiles. Turbulent velocity scales (u_s) were approximated by the locally measured Reynolds shear stress, such that $u_s = (\tau_{RS}/\rho)^{1/2}$. This definition of u_s is similar to that of the friction velocity (u_*) which is often used to parameterize bed shear stresses in unobstructed boundary layer flows (e.g. Cannon and Troy, 2018; Whitman and Reidenbach, 2012). However, unlike u_* it should be noted that u_s cannot be used to infer bed stress since $\overline{u'w'}$ is unlikely to follow canonical boundary layer scaling, especially within the oyster canopy where turbulence is generated by a combination of bed shear and flow interactions with individual oyster clusters. While the appropriate velocity scale for turbulent mixing and mean flow in canopies is unclear (e.g. Kastner-Klein and Rotach, 2004), the locally measured Reynolds stress (τ_{RS}) is a natural turbulence scaling parameter commonly used in both canonical boundary layer flows (e.g. Wüest and Lorke, 2003) and canopy flows (e.g. Reidenbach et al., 2006; Styles, 2015). Turbulence characteristics were therefore normalized by local turbulent velocity scales (u_s) to facilitate comparisons between reefs.

Turbulent kinetic energy dissipation rates (ϵ) were estimated from vertical velocity time series (120 s; 50% overlapped) using a wave-corrected second order structure function. This method allows for robust dissipation estimates in the presence of surface waves, since wave fluctuations are effectively removed when the structure function is computed using simultaneous, vertically separated turbulence time signals. Best-fit dissipation estimates were calculated following the least-squares approach outlined in Scannell et al. (2017), who define the wave-corrected second order structure function as:

$$D_{LL}(x,r) = \left\langle [w(x+r/2) - w(x-r/2)]^2 \right\rangle = A_o + C_2\epsilon^{2/3}r^{2/3} + A_3\left(r^{2/3}\right)^3$$

where r is the vertical separation distance between measurements centered on location x, C_2=2.1 is a universal constant of proportionality (e.g. Wiles et al., 2006), A_3 is a fit constant that represents the contribution of wave orbital motion, and A_o is a coefficient representing the contribution of Doppler noise, estimated in this study using the methods of Thomas et al. (2017). Fits were conducted using a centered differencing scheme with velocity measurements centered on the profile midpoint and collected in the constant-noise portion of the sample volume (i.e. midpoint±5 mm), resulting in a total of 5 points used for each fit. Fits with adjusted R^2 values (e.g. Scannell et al., 2017) less than 80% were rejected as erroneous. Importantly, dissipation rates estimated using wave-corrected second order structure functions compared favorably with those calculated using spectral fitting techniques (i.e. Trowbridge and Elgar, 2001; $R^2 > 90\%$), although spectral fitting was limited due to strong surface wave contamination ($0.3 < f < 2$ Hz) in the inertial subrange.

3. Results

3.1. Oyster reef morphology

Morphology of restored and reference reefs were similar, with no apparent trend across restoration age, while vertical structure of the degraded reef diverged considerably. Maximum crest elevations of restored and reference reefs varied from 10 to 30 cm below NAVD 88, with crest widths between 4 and 20 m (Fig. 2) which were fully inundated during all experiments. By contrast, the crest of the degraded reef was nearly 30 cm above the highest live reef elevation, placing it well above both the mean water level and the inundation threshold for successful oyster recruitment (Ridge et al., 2015). Importantly, the degraded reef was never fully inundated during the study.

Oyster canopy in restored reefs was well-developed and largely comparable to the reference reef, even in the reef that had been restored within one year of the study (Fig. 3; Table 1). Live oyster densities tended to be greater in the restored reefs (208–475 oysters/m^2) as compared to the reference reef (184 oysters/m^2), but manual counts of solid elements (which include both live oyster and non-living reef structure) were 75–100% greater in the reference reef, reflecting longer-term growth patterns of oyster recruitment and senescence. Mean reef-wide canopy height and solid volume fraction estimates were similar in the two younger restored reefs and the reference reef, varying between 5.5 and 6.0 cm and 7.5–7.6%, respectively. The tallest and densest canopy structure (h_s: 8.3 cm, SVF: 10.7%) was observed on the oldest restored reef (R-2014), where live oyster densities were also greatest (475 oysters/m^2). Importantly, canopy heights were well correlated between different estimation methods, with less than 1 cm of difference between estimates based on manual measurement and laser scans. In all reefs, canopy characteristics varied spatially, with patchy clusters of dense oyster growth driving regionally high solid volume fraction and canopy height estimates. Canopy heights were typically largest on the reef fringes, especially for the R-2016 and Reference reefs, where canopy heights were 2–5 times larger on the reef edge than in the reef interior.

3.2. Reef hydrodynamics

3.2.1. Tidal currents and wave energy

Water depths, channel-to-reef velocity gradients, and wave attenuation were similar in restored and reference reefs and no clear trend related to restoration age was detected. Canopies of restored and reference reefs were submerged during all experiments, with an average crest submergence depth of 20 cm during near-bed measurements and 35 cm during above-canopy measurements (Fig. 4a,b). The water depth

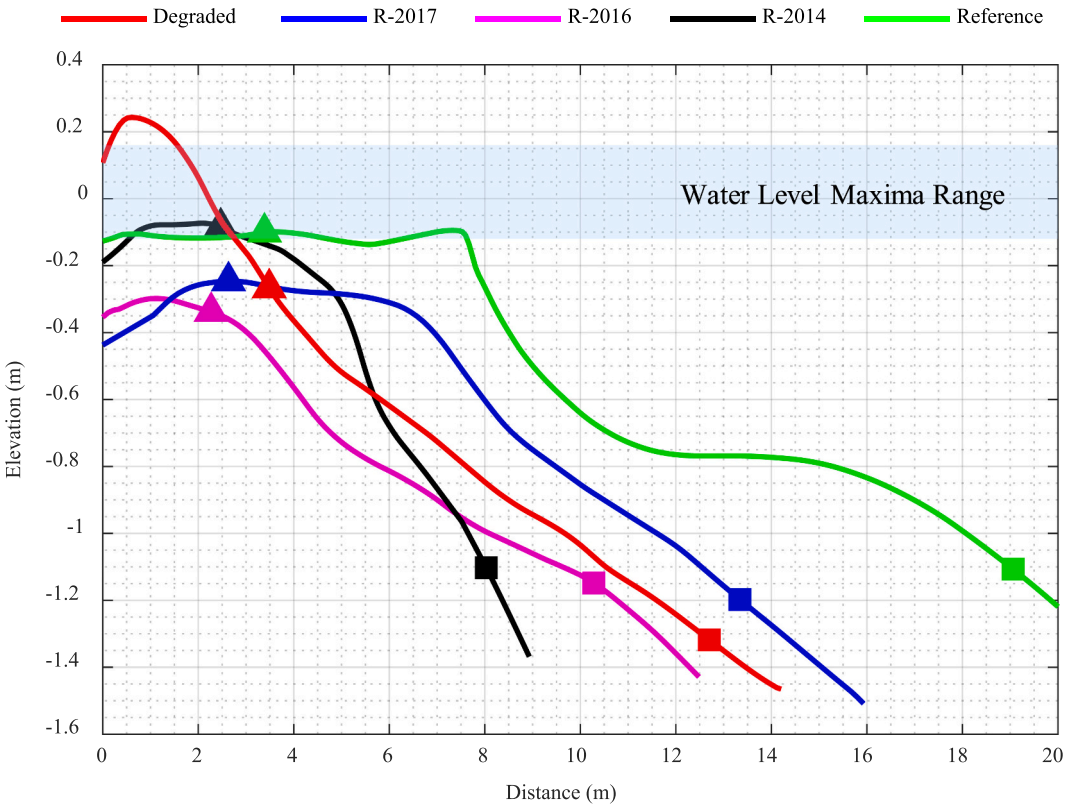

Fig. 2. Cross-sectional reef elevation profiles. Lines are colored by reef name and markers represent the locations of velocity profiles measured on-reef (triangle) and in the channel (square). The blue band represents the range of observed water level maxima at all reefs. (For interpretation of the references to colour in this figure legend, the reader is referred to the web version of this article.)

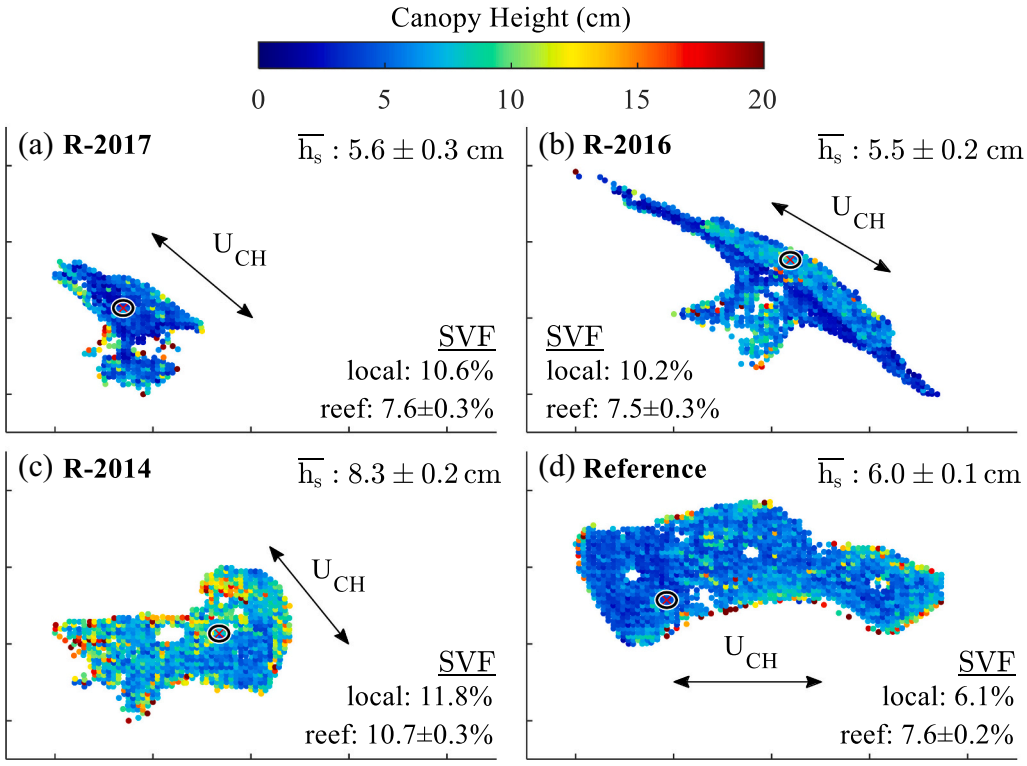

Fig. 3. Oyster canopy height (h_s) and solid volume fraction (SVF) estimated from high-resolution surface scans for the (a-c) restored and (d) reference reefs. The direction of streamwise channel flow (U_{CH}) at each reef is indicated with double headed arrows (15 m length), and the position of on-reef velocity measurements is shown as an open circle (diameter: 2 m). Reef-wide canopy height averages are included for reference ($\bar{h}$: mean ± 95% CI). SVF averages are calculated over the entire reef surface (reef) and in the immediate vicinity (1 m radius) of the velocity probe (local). All reefs are drawn to the same scale.

never exceeded the crest elevation at the degraded reef, creating a hydraulic disconnect between the channel and reef backwaters and a local flow stagnation boundary at the reef. Significant wave heights measured in the channel were typically less than 5 cm, with an average wave height of 2 cm across all experiments. Waves were weakly attenuated as they passed from the channel over the reefs, with an average wave height attenuation of 25±12% over all experiments (Fig. 4c,d). Although wave heights were small, waves were still hydrodynamically important (Fig. 5). The spectral signature of surface waves was evident in almost all velocity time series, with wave energy contributions increasing as reef velocity and water depth decreased. Waves were particularly influential to the energy balance when significant wave height exceeded 10% of the water depth over the reef and when the depth-integrated channel velocity was less than 7.5 cm/s.

Velocities measured in and above the reef canopy were considerably lower than in the adjacent channel and demonstrate the variability of hydrodynamic habitat niches within oyster canopies. Depth-integrated channel velocities were similar across sites and varied over the tidal cycle, with the strongest velocities (10–25 cm/s) measured during times of peak tidal exchange (Fig. 4e,f). Near-bed current speeds measured within the oyster canopy (~2 cmab, Fig. 4e) ranged from 0.5–4 cm/s. Above-canopy (9.5 cmab) current velocities (Fig. 4f) were generally 3 to 5 times greater than those measured near the bed, a function of both the elevated position within the bed boundary layer and the diminished oyster canopy interaction. While there were slight differences in channel-to-reef velocity attenuation among restored and reference reefs (84–97% near-bed and 51–65% above-canopy; Fig. 6; Table 2), attenuation rates did not vary predictably with canopy metrics or restoration age. Although there was a significant linear relationship between flow speeds measured on and off the reef at reference and restored sample sites, there was no significant relationship between channel velocities and velocities measured on the degraded reef. This disconnection reflects how reef morphology, particularly the lack of crest inundation, influenced local hydrodynamics at the most fundamental level.

3.2.2. *Turbulence characteristics*

Turbulence generally scaled with the local velocity, such that higher velocities were associated with enhanced mixing rates. The highest mixing rates were observed above the oyster canopy, with mean vertical turbulent energy ($\overline{w'^2}$; Fig. 7a), turbulent kinetic energy dissipation (ϵ; Fig. 7b), and turbulent shear production (P; Fig. 7c) estimates ranging from 10^{-4}–10^{-3} m^2/s^2 ($\overline{w'^2}$) and 10^{-5}–10^{-4} m^2/s^3 (ϵ, P), respectively. In all reefs, turbulence characteristics measured within the canopy were considerably more variable than those measured above the canopy. Near-bed turbulence characteristics were significantly greater within canopies of restored or reference reefs than above the degraded reef, with order of magnitude enhancements in both turbulent energy (10^{-5} vs. 10^{-6} m^2/s^2) and turbulent kinetic energy dissipation (10^{-6} vs. 10^{-7} m^2/s^2) despite statistically similar current magnitudes (0.70±0.10 cm/s vs. 0.75±0.05 cm/s). The same trend was observed for turbulent production, with average near-bed production estimates that were 10–100 times greater above live versus degraded oyster reefs.

Turbulence characteristics of restored reefs were similar to the reference reef, regardless of restoration age. Normalized turbulent energy and dissipation estimates (Fig. 7d,e) converged across restored and reference reefs for both near-bed and above-canopy observations. When normalized by the local velocity scale (u_s), median dimensionless turbulent energy estimates ($\overline{w'^2}/u_s^2$) converged across restored and reference reefs to 1.5 ±0.1 for above-canopy flows and 1.6±0.3 for near-bed flows. Turbulent kinetic energy dissipation was similarly well represented by wall scaling (e.g. Cannon and Troy, 2018), where within- and above-canopy estimates were scaled by $u_s^3/\kappa z$, with κz used as a bed-distance length scale, κ=0.41 (i.e. von Karman's constant), and z defined as the measurement distance above the bed. Wall scaling tended to overpredict observed dissipation rates, with a normalized average of 0.50±0.03 and 0.30± 0.05 for above- and within-canopy flows, respectively. In terms of the energy budget, average turbulent production was generally much larger than turbulent dissipation at the restored and reference reefs, with P/ϵ ratios ranging from 2 to 5 (Fig. 7f). By contrast, the turbulence budget was more balanced at the degraded reef,

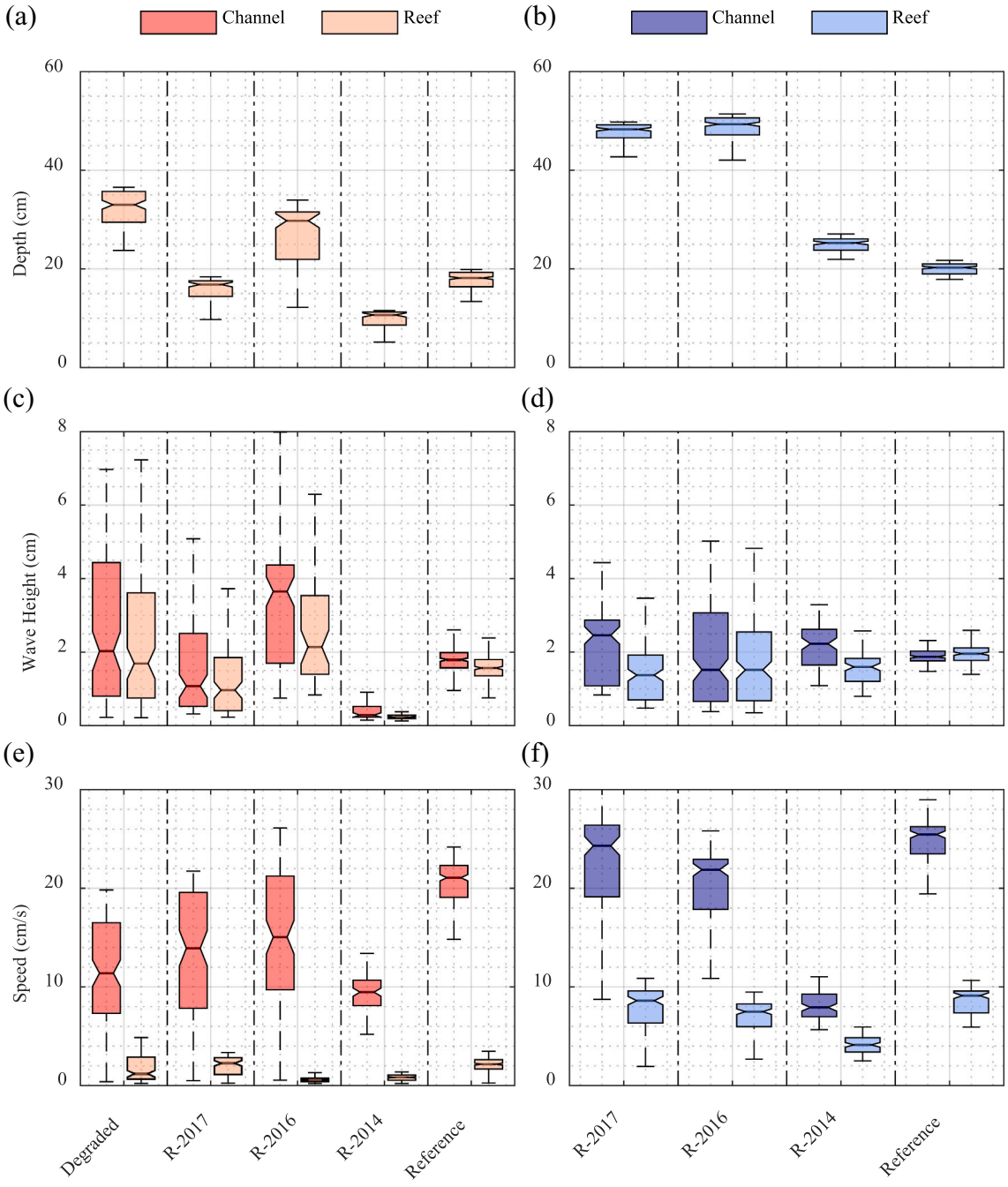

Fig. 4. Hydrodynamic characteristics observed over each experiment, including (a,b) water depth above the reef crest, (c,d) channel and on-reef measured wave heights, and (e,f) channel and on-reef measured horizontal current speeds for both near-bed (a,c,e) and above-canopy (b,d,f) experiments. Box plots indicate the median (center line), 25th percentile (top edge), and 75th percentile (bottom edge), with whiskers extending to the most extreme data points. Outliers have been removed. 95% confidence intervals on sample medians are displayed as notches along the side of each box.

where 95% confidence intervals on the average P/ϵ ratio included unity (1.5 ± 0.5).

Comparisons of turbulent velocity scales normalized by the on-reef current speed reveal similar hydrodynamic behavior in restored and reference reef. Within the canopy, normalized velocity scales varied as a function of current speed, with multiple order enhancements in u_s^2/U_R^2 observed at low flow velocities (Fig. 8a). Although average estimates of u_s^2/U_R^2 on restored and reference reefs varied by over two orders of magnitude ($\overline{u_s^2/U_R^2}$: 0.071–0.418), differences were largely related to the reef current speed, with higher estimates of u_s^2/U_R^2 observed on reefs with strong flow attenuation (i.e. R-2016 and R-2014). While near-bed estimates of u_s^2/U_R^2 on reference, restored, and degraded reefs were similar (O[10^{-1}]) at the lowest flow speeds (5 mm/s $< U_R <$ 10 mm/s), u_s^2/U_R^2 estimates at higher current velocities were significantly lower on the degraded reef (O[10^{-3}]) than those observed within live oyster canopies (O[10^{-2}]). Above the canopy, u_s^2/U_R^2 estimates (Fig. 8b) were significantly lower than within the canopy, with average magnitudes ranging from 0.028 ± 0.001 (R-2017) to 0.056 ± 0.004 (R-2014). The influence of current speed was nearly negligible above the oyster canopy, and u_s^2/U_R^2 estimates across restored and reference reef converged above 3 cm/s (>95% of all measurements).

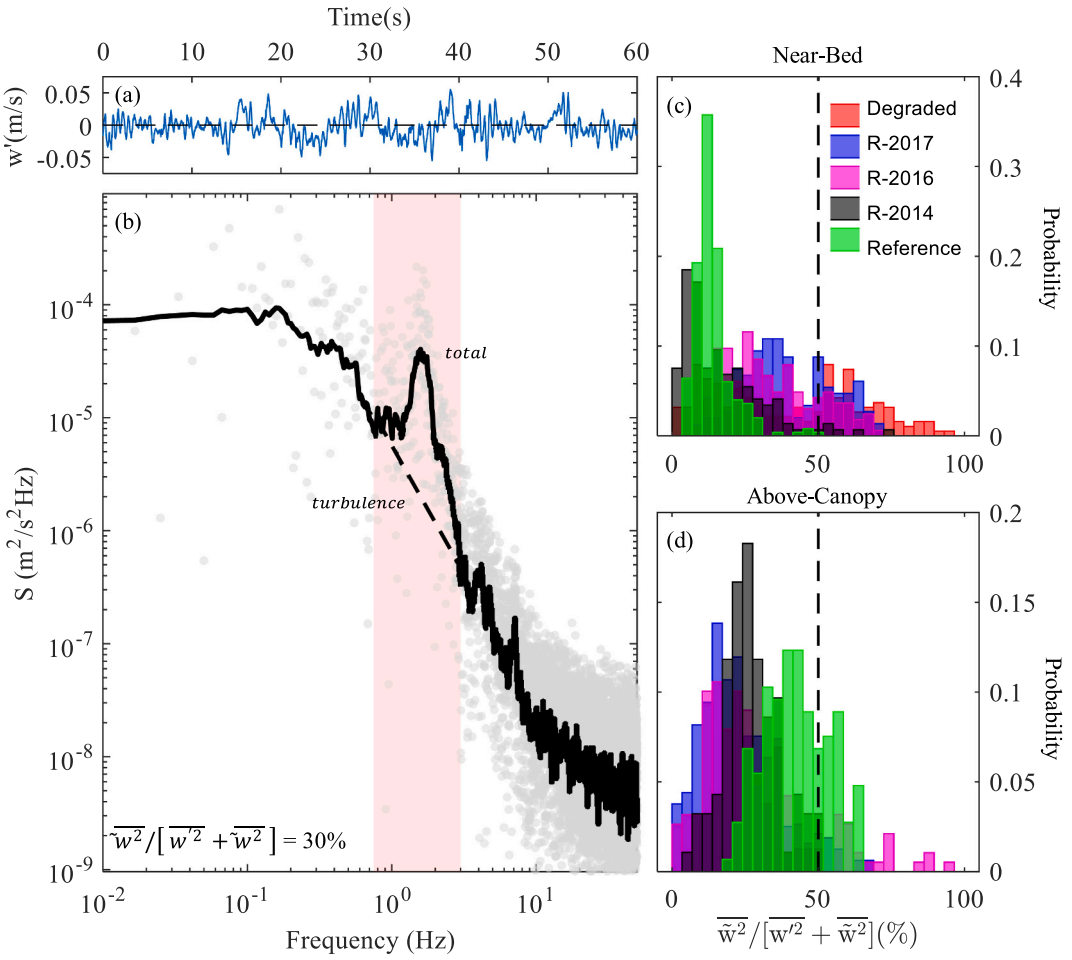

Fig. 5. Summary of wave energy influence over sampled oyster reefs. Energy spectra (b) computed from time series of vertical velocity fluctuations (a) are used to separate turbulence spectra (dashed line, 25 pt. smoothed) from the total wave+turbulence spectra (solid line, 25 pt. smoothed). Histograms are used to show the total contribution of wave energy estimated over each 120 s data segment observed during the near-bed (c) and above-canopy (d) experiments.

4. Discussion

From a hydrodynamic perspective, restored oyster reefs in Mosquito Lagoon, Florida were comparable to live reference reefs within a relatively short time following restoration. High-resolution hydrodynamic data collected under a variety of forcing conditions above and within the oyster canopy indicated that live reference and restored reef hydrodynamics were functionally similar less than one year after restoration (i.e. one recruitment cycle), the shortest time frame considered in the study. Comparisons across reefs of varied restoration ages suggested that the transition from degraded to functionally live reef was a nonlinear threshold response near the time of restoration, as opposed to a continuum of hydrodynamic characteristics that shifted gradually over years (multiple recruitment cycles) since restoration. However, the dataset also revealed functional differences in canopy-flow interaction unique to each reef and suggested causal mechanisms which may explain the observed variability. While channel-to-reef velocity attenuation and turbulence were fairly consistent above the reef canopy, where the entire reef structure can be treated like a single roughness element (e.g. Styles, 2015), within-canopy hydrodynamics were far more variable, with statistically significant differences in mean velocity attenuation that resulted in order of magnitude variability in average normalized turbulent velocity scales (u_s^2/U_R^2) at each reef. The consistency of hydrodynamic characteristics above the oyster canopy suggests that the near-bed variability was not due to variations in bulk reef morphology (i.e. reef slope, reef shape, crest elevation, topography), but rather reef-specific canopy characteristics.

4.1. Reef structure

High resolution laser-scans revealed considerable variability of surface roughness and canopy height within reefs and highlighted spatial patterns of oyster growth that were consistent among restored and reference reefs. While correlated with live oyster density, the canopy characteristics detected by surface scans represented an amalgamation of canopy structure created by both living oyster and the shells of deceased oyster upon which the reef was built. Whereas canopy characteristics were similar across both reference and restored reefs (h_s: 5.5–8.3 cm; SVF: 7.5–10.6%), at smaller spatial scales the reef surfaces were highly heterogeneous, with canopy heights in individual 0.5 m computation grids often exceeding 15 cm. This heterogeneity partially reflects the oyster canopy formation habit into semi-isolated clusters, which have more in common with a canopy of vegetation than a homogeneous carpet over the bed. However, larger-scale growth patterns were also apparent. For instance, dense, tall oyster structures were especially pronounced on reef margins (see R-2016 and Reference reefs), while canopy heights in reef interiors were consistently below the reef average. This pattern indicates active oyster growth and reef expansion at the margins (Ridge et al., 2015) and potentially preferential recruitment to reef edges. Within-reef surface heterogeneity is expected to have significant impacts on mean flow and mixing within the reef canopy, with variability in canopy structure leading to local alterations in both

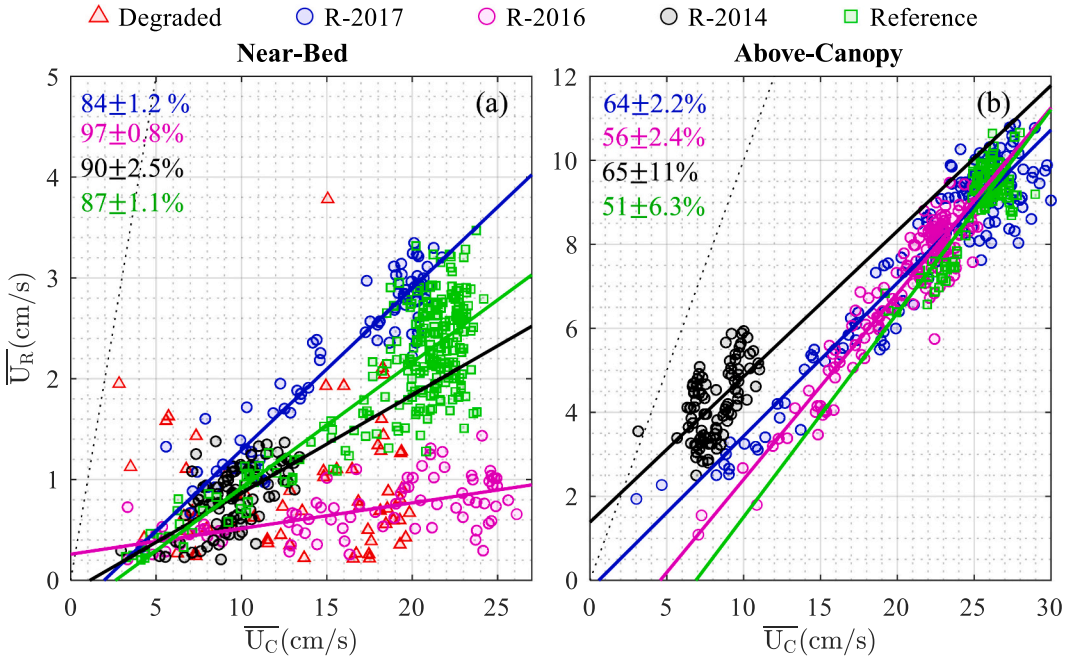

Fig. 6. Velocity attenuation from channel to reef as observed (a) near-bed (2cmab) and (b) above the oyster canopy (9.5 cmab). Best-fit linear models (robust fitting) are shown for fit slopes that were significant at the 95% confidence level ($p < 0.05$). 1:1 lines (black; dotted) are included for reference and represent 0% velocity attenuation.

flow paths and turbulence production. This likely explains the variability of within-canopy hydrodynamics observed in this and prior studies of spatially heterogeneous submerged canopy flows (e.g. Davis et al., 2021). R-2016 provides some evidence for this hypothesis, with observations of strong velocity attenuation and elevated normalized turbulent velocity scales (u_s^2/U_R^2) linked to the measurement location in the transition between regions of high (SVF > 10%; h_s>10 cm) and low (SVF < 5%; h_s<5 cm) oyster canopy densities.

4.2. Mixing characteristics

Turbulence characteristics observed in the restored and reference reefs agree well with previous reports of mixing in shallow estuarine canopy flows. Observed turbulent kinetic energy dissipation rates (ϵ) were on the order of 10^{-6} and 10^{-5} m^2/s^3 for near-bed and above-canopy flows, respectively, with commensurate vertical turbulent energy estimates on the order of 10^{-5} and 10^{-4} m^2/s^2. These values parallel previous estimates for intertidal oyster reefs in Mosquito Lagoon (Kitsikoudis et al., 2020), where turbulence characteristics at the highly energetic ($U_R \approx$ 10 cm/s) canopy-flow interface were estimated as O (10^{-4}) for dissipation and O(10^{-3}) for turbulent kinetic energy. Styles (2015) observed slightly stronger mixing rates above an oyster canopy in North Inlet, South Carolina (ϵ: 10^{-4} - 10^{-3} m^2/s^3; turbulent kinetic energy (k): 10^{-4} - 10^{-3} m^2/s^2), though measured current speeds were over twice as large (U_{max}: 30 cm/s) as those observed in the current study. Above-canopy measurements herein also agree with other reported biological canopy flows, including coral reefs (e.g. Reidenbach et al., 2006; ϵ : 10^{-5} m^2/s^3; k:10^{-4} m^2/s^2), red mangrove prop roots (e.g. Kibler et al., 2019; ϵ : 10^{-6} m^2/s^3; k:10^{-3} m^2/s^2), and submerged seagrass canopies (e.g. Hansen and Reidenbach, 2017; ϵ : 10^{-5} m^2/s^3; k:10^{-3} m^2/s^2). Notably, average turbulence characteristics measured near the bed on the degraded reef (ϵ : 10^{-7} m^2/s^3; k:10^{-6} m^2/s^2) were significantly weaker than those measured on the restored or reference reefs investigated in this study, with magnitudes that agreed better with low-energy flows over rough shell boundaries (Cannon and Troy, 2018: ϵ: 10^{-7} m^2/s^3; k:10^{-6} m^2/s^2).

Near-bed turbulence characteristics were highly variable, with multi-order fluctuations in both turbulent energy ($\overline{w'^2}$: 3×10^{-6}–2×10^{-4} m^2/s^2) and turbulent kinetic energy dissipation (ϵ:1×10^{-7}–6×10^{-5} m^2/s^3). Individual reefs experienced dramatic fluctuations in near-bed mixing (1–2 orders of magnitude in ϵ and $\overline{w'^2}$) over the course of a single flood tide. Importantly, similar variability was not observed in turbulence measurements above the canopy ($\overline{w'^2}$: 8×10^{-5}–7×10^{-4} m^2/s^2; ϵ: 3×10^{-5}–2×10^{-4} m^2/s^3), despite similar forcing characteristics (i.e. channel/on-reef velocities, waves, water levels). This variability agrees well with theories and observations related to turbulence generation in complex canopy structures (e.g. Monismith, 2007; Davis et al., 2021). Namely, within reef mixing is considerably more complicated than typical boundary layer flows, with canopy induced vortex shedding, reef heterogeneity, and turbulent injections from both the bed and canopy surface leading to dramatic temporal and spatial variations in within canopy turbulence (Davis et al., 2021).

4.3. Turbulence budget

Non-equilibrium turbulence budgets were observed both above and within the oyster canopy of all live reefs. For above-canopy flows, turbulent shear production (P) was on average 3–4 times greater than turbulent dissipation (ϵ), with consistent P/ϵ ratios observed across both reference and restored reefs. This agrees well with previous studies of flow above submerged canopies, where P/ϵ ratios greater than unity were reported for oyster reefs (Kitsikoudis et al., 2020), coral reefs (Reidenbach et al., 2007), and plant canopies (Finnigan, 2000). This imbalance in the above-canopy turbulence budget is typically attributed to enhanced production in the shear layer at the canopy-flow interface (e.g Reidenbach et al., 2007), which is a reasonable hypothesis in the current work given the location of the sampling volume within 2–3 cm of the canopy surface. It's important to note that a persistent canopy shear layer, as observed in flows through submerged vegetation (Nepf, 2012), is unlikely to develop above heterogenous oyster canopies where individual flow-body interactions may have sufficient room to recover between oyster clusters. However, the canopy structure likely induces enhanced shear at the canopy-flow interface, even if the shear layer itself

Table 2
Summary of hydrodynamics (mean ±bootstrapped 95% confidence intervals) observed over each experiment: mean horizontal current speeds ($\overline{U_R}$, $\overline{U_C}$), mean significant wave heights (H_s), and total wave energy contributions ($\overline{\tilde{w}^2}/[\overline{w'^2}+\overline{\tilde{w}^2}]$), on the reef (*) and in the channel (^). Estimates of the channel-to-reef velocity and wave attenuation (%) are shown in square brackets ([]) when relationships are significant ($p<0.05$). The percentage of data discarded due to excess wave energy ($\overline{\tilde{w}^2}/[\overline{w'^2}+\overline{\tilde{w}^2}]>50\%$) is also reported ({}).

Reef name	Current speed (cm/s)		Wave height (cm)		Wave energy contribution $\overline{\tilde{w}^2}/[\overline{w'^2}+\overline{\tilde{w}^2}]$ (%)	
	Near-Bed	*Above-Canopy*	*Near-Bed*	*Above-Canopy*	*Near-Bed*	*Above-Canopy*
Degraded	1.0 ± 0.1* 14 ± 2.3^ [$p \gg 0.05$]	–	0.9 ± 0.3* 1.0 ± 0.3^ [11 ± 2.9%]	–	41 ± 5.0* {44%}	–
R-2017	2.2 ± 0.2* 16 ± 1.0^ [84 ± 1.2%]	8.0 ± 3.7* 22 ± 1.0^ [64 ± 2.2%]	0.9 ± 0.2* 1.2 ± 0.2^ [28 ± 2.2%]	1.4 ± 0.1* 2.2 ± 0.2^ [36 ± 4.3%]	40 ± 2.3* {31%}	22 ± 2.1* {4.5%}
R-2016	0.7 ± 0.1* 17 ± 1.5^ [97 ± 0.8%]	7.1 ± 0.2* 21 ± 0.6^ [56 ± 2.4%]	2.5 ± 0.4* 2.7 ± 0.3^ [−4.4 ± 3.7%]	1.6 ± 0.2* 1.7 ± 0.2^ [9.2 ± 1.7%]	34 ± 2.4* {20%}	28 ± 2.7* {15%}
R-2014	0.8 ± 0.1* 9.6 ± 0.4^ [90 ± 2.5%]	4.2 ± 0.2* 8.2 ± 0.3^ [65 ± 11%]	0.3 ± 0.0* 0.4 ± 0.2^ [58 ± 3.2%]	1.5 ± 0.1* 2.2 ± 0.1^ [33 ± 6.6%]	17 ± 2.1* {3.5%}	27 ± 2.0* {2.2%}
Reference	2.1 ± 0.1* 19 ± 0.6^ [87 ± 1.1%]	8.9 ± 0.2* 25 ± 0.3^ [51 ± 6.3%]	1.6 ± 0.1* 1.8 ± 0.1^ [49 ± 7.8%]	1.9 ± 0.1* 1.8 ± 0.1^ [5.8 ± 15%]	14 ± 0.8* {0%}	43 ± 1.8* {25%}

is transient.

Average turbulent shear production rates were also significantly greater than dissipation rates ($P/\epsilon \approx 1$–5) for all within-canopy measurements collected near the bed, although individual estimates of P/ϵ varied by more than an order of magnitude ($0.5 < P/\epsilon < 10.5$). This variability is indicative of the complex turbulence budget within the canopy, where bed friction, structure induced vortex shedding, and downstream turbulence transport all play significant roles in turbulence generation (Davis et al., 2021). In fact, the true P/ϵ ratios for flows within oyster canopies are likely even larger than those reported here, since we were unable to estimate the contribution of cluster-induced wake production in the full turbulence budget. While similar imbalances in dissipation and production have been reported within the canopy on oyster reefs (Kitsikoudis et al., 2020), these results disagree with many studies focused on flow through submerged vegetation, where production (or, more accurately, $\overline{u'w'}$) is often considered negligible within dense canopy structures (Nepf, 2012). This disagreement highlights the functional differences between structurally complex oyster canopies, where flow velocities are weak but persistent, and dense vegetation canopies, where horizontal momentum is negligible. Although we cannot reliably disentangle the terms of the turbulence budget in the current work, we can state with confidence that turbulence production and dissipation are likely non-zero and non-equilibrium ($P > \epsilon$) for within-canopy flows, and that turbulence budgets in restored reef are similar to reference reef. Furthermore, observations of near-bed production and dissipation at the degraded reef illustrated that the turbulence budget was, on average, in equilibrium ($P \approx \epsilon$), with 95% confidence intervals on the median ratio of P/ϵ including unity. This supports the hypothesis that vertical oyster structures enhanced production on the reference and restored reefs, while production at the degraded reef was primarily generated through bed friction over the rough boundary.

4.4. Normalized turbulent velocity scales

In the current study, normalized turbulent velocity scales measured above the reef (Fig. 8b; u_s^2/U_R^2=0.028–0.040) agreed well with previous reports of drag ($C_d = u_*^2/U^2$) above submerged canopies. For flows above rigid biological canopies, where the canopy structure can be treated like a large roughness element, the friction velocity (u_*) is often parameterized using Reynolds stress methods similar to those used for estimating u_s in the current study (e.g. Reidenbach et al., 2006; Styles, 2015), allowing for reasonable comparisons between C_d and u_s^2/U_R^2. Styles (2015) reported similar drag coefficients at ~10 cmab (i.e. above the bed) on intertidal oyster reefs (*C. virginica*), with an estimated C_d=0.031. Reidenbach et al. (2006) also observed comparable drag coefficients above a coral reef, where elevation-corrected C_d ranged from 0.040–0.153 at 10 cmab (C_{d-1m}=0.009–0.015).

Following the work of Styles (2015), Nikuradse roughness heights (k_s) were estimated from normalized velocity scales, such that $k_s \approx 30ze^{-\kappa U_R 2/u_s 2}$. Near-bed estimates of u_s^2/U_R^2 at the degraded reef (Fig. 8a; $\overline{u_s^2/U_R^2}$=0.011 ± 0.004) produced an average roughness height of $\overline{k_s}$=1.0 cm, a value that was well correlated with the median diameter (D_{50}) of surface particles at the sample site. Commensurate roughness heights above the canopy on reference and restored reefs ranged from 26 to 53 cm, with an average roughness-to-canopy height ratio ($\overline{k_s/h_s}$=5.7) supporting the results of Styles (2015), who found that the equivalent roughness was between 3 and 6 times the canopy height on a natural intertidal oyster reef. Most importantly, estimates of $\overline{u_s^2/U_R^2}$ and $\overline{k_s/h_s}$ show that flows above the canopy on restored reefs have similar turbulence characteristics to those observed above natural reefs within 1 year of restoration.

Within-canopy estimates of u_s^2/U_R^2 generally decreased with on-reef current speed (Fig. 8a). Although mean estimates of u_s^2/U_R^2 varied by an order of magnitude within the canopy on reference and restored reefs (0.071–0.418), all measurements displayed comparable speed dependencies, suggesting that variations were not linked to fundamental differences in turbulence generation. We hypothesize that the low-speed enhancements in u_s^2/U_R^2 observed in the current work can be attributed to the vertical and horizontal advection and diffusion of turbulence across the heterogeneous canopy structure. This advected turbulence would not scale with the local velocity, as described by u_s^2/U_R^2, but rather with velocities measured above the canopy, upstream of the measurement location, or outside the canopy at the channel-reef fringe. A more detailed analysis of turbulent flow in submerged oyster canopies is beyond the scope of this study, but future work on oyster reefs should focus on parameterizing the spatial structure of the flow field to gain a better understanding of the appropriate scaling parameters and turbulence budget, especially within the canopy.

4.5. Implications for oyster reef restoration

This study suggests that the hydrodynamic characteristics of properly restored and intact oyster reefs may be functionally similar shortly after restoration, with transformations observed within six months of restoration in the current work. These results support the practice of oyster reef restoration to restore hydrodynamically mediated ecosystem services (e.g. shoreline protection, sediment retention, etc.) associated

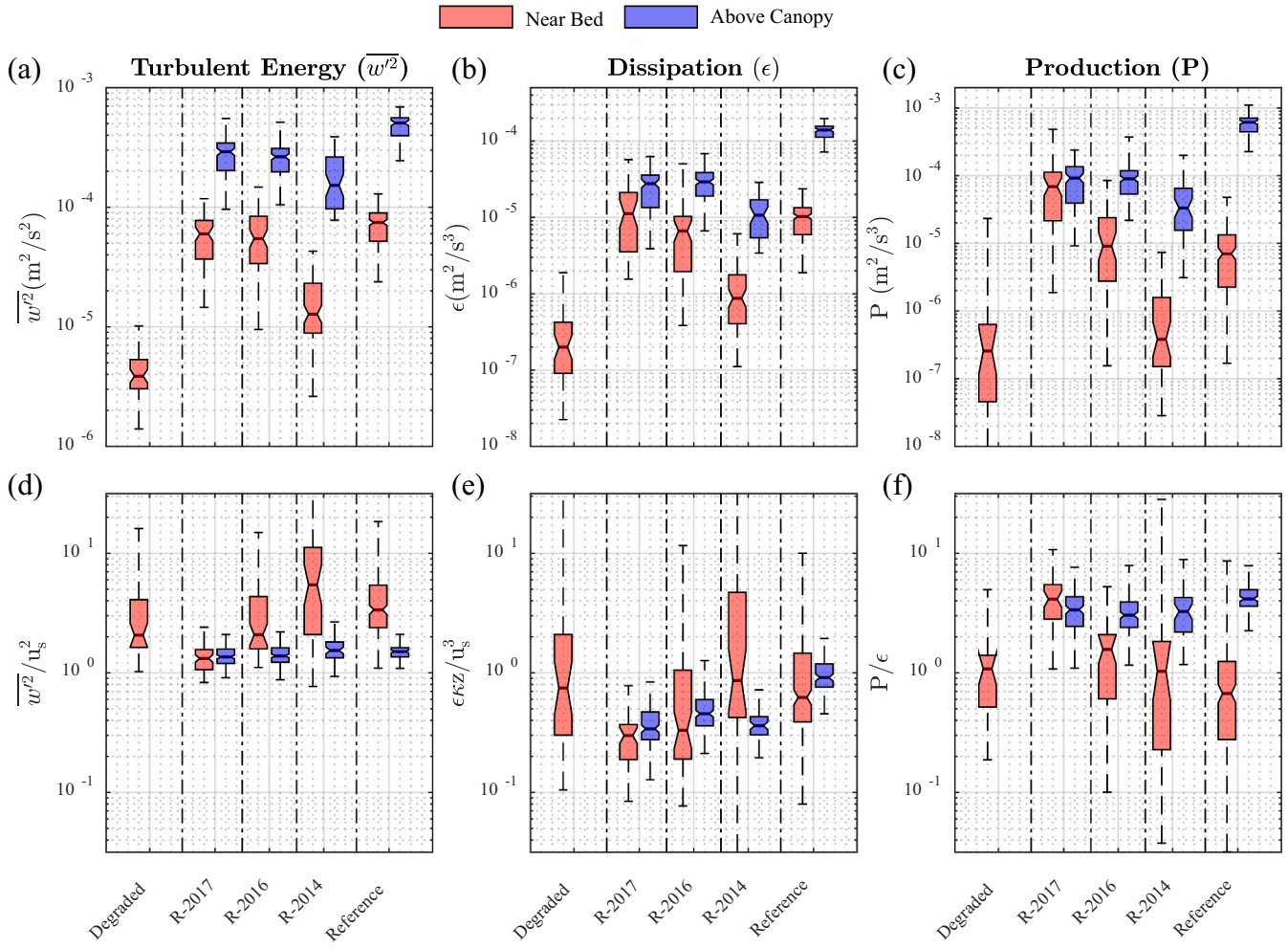

Fig. 7. Raw (a,b,c) and normalized (d,e,f) turbulence characteristics for measurements collected near the bed (red) and above the canopy (blue). Turbulent energy (a; $\overline{w'^2}$) is normalized (d) by the locally estimated velocity scale (u_s), while dissipation (b; ϵ) is normalized (e) by the wall estimate ($u_s^3/\kappa z$). Turbulent production (c; P) is normalized (f) by dissipation in order to investigate differences in the turbulent kinetic energy budget. All turbulence characteristics were estimated using wave-turbulence decomposition such that the given values are free of surface-wave bias. Box plot descriptions are included in Fig. 4. (For interpretation of the references to colour in this figure legend, the reader is referred to the web version of this article.)

with healthy oyster reefs. Furthermore, the fundamentally different flow patterns observed around live and degraded reefs highlight the critical influence of live oyster canopy and biologically-mediated structural controls to hydrodynamic and geomorphic processes. Frequency of submergence, as determined by reef elevation, had significant implications to hydrodynamics and therefore to shoreward energy and nutrient fluxes. While the live intertidal reefs facilitated flow across the reef surface for at least a portion of each tidal cycle, the degraded reef was a consistent stagnation point in the flow field, acting as a barrier to transport between the main channel and the reef backwater, potentially reducing, or completely eliminating, cross-reef nutrient and momentum fluxes (Stiner and Walters, 2008).

The crest elevation of live reefs is set by controls to oyster recruitment and growth (e.g. water surface elevation, inundation times: Rodriguez et al., 2014). In the absence of living oyster, degraded reef elevations are determined solely by local hydrodynamic pressures (e.g. wave and current magnitudes) and the bulk stability of disarticulated shells (Grizzle et al., 2002; Walters et al., 2007; Garvis et al., 2015). Lacking recruitment, degraded reefs will evolve through geomorphic processes, initially heightening and steepening as observed herein, and eventually eroding. Although degraded reefs may offer landward shoreline protection (McClenachan et al., 2020) and sediment retention in the short term (i.e. as the degraded reef migrates and collapses; ~1 m/yr migration rate: Garvis et al., 2015), hydrodynamic influences of cross-reef wave reduction or current attenuation are likely transient, and accompanied by reductions in nutrient and oxygen renewal on the shoreward side of the reef.

The structural and hydrodynamic similarity observed between the reference and restored reefs discussed in this study should be considered in the context of both restoration technique and oyster recruitment potential. For instance, these results contrast with other recent work on restored *C. virginica* oyster reefs in the mid-Atlantic (i.e. Whitman and Reidenbach, 2012), where dramatic hydrodynamic differences were observed above intact reference reefs and reefs that were recently restored (restoration age: ~1 yr) using deposited flat-stacked oyster shells. We hypothesize that the restorations studied in this work were more successful at quickly replicating the flow dynamics of intact reefs due to: (1) restoration technique, in particular the use of oyster mats designed to mimic vertical reef structure (Garvis et al., 2015); and (2) prolific oyster recruitment, linked to both the mat structure and the extended growing season in Mosquito Lagoon (April to December, L. Walters pers. obs.). Although the oyster mats created a spatially sparse canopy at the time of deployment, extensive oyster recruitment was required for solid volume fractions and canopy heights to reach levels similar to intact reference reefs. This suggests that the observed flow effects were not caused by the mats themselves, but rather by the rapid

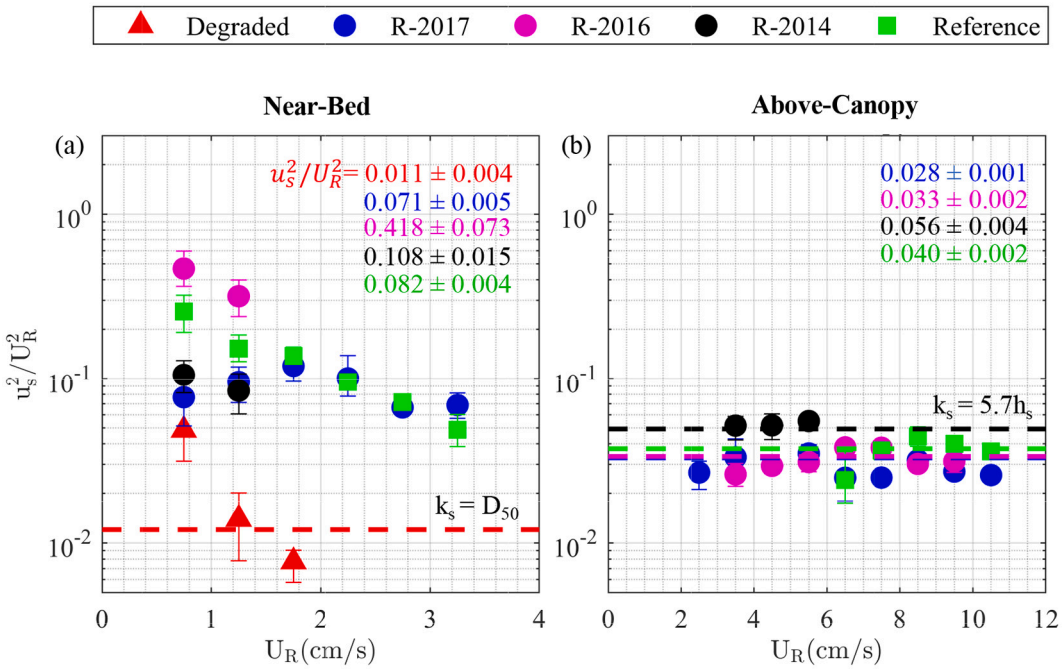

Fig. 8. Turbulent velocity scales (u_s^2) normalized by on-reef current speeds (U_R^2) for near-bed (a) and above-canopy (b) experiments. Normalized velocity scales (colored markers: mean ± 95% CI) are averaged over constant-width velocity windows (a: 0.5 cm/s; b: 1 cm/s). Dashed horizontal lines show the theoretical drag coefficients ($C_d = \kappa^2/\log(30z/k_s)^2$) for flow above disarticulated shells ($k_s = D_{50}$) and rigid oyster canopies ($k_s = 5.7h_s$). The average turbulent velocity scale ratios computed using all measurements collected during each experiment are included for reference (colored text; mean ± 95% CI).

colonization of oyster spat that attached and grew on them. The link between oyster recruitment and hydrodynamic response time means that changes are predicated on successful spat attachment and growth. As such, restoration projects in estuaries where oyster populations have been impacted by pollution, acidification, or disease are likely to see longer response times, or no response at all, especially if the problems remain unmitigated. It is also possible that oyster reef restorations attempted using different restoration techniques or in estuaries with less productive oyster communities may see a slower hydrodynamic response time.

5. Conclusions

For this study, in-situ field experiments were used to compare the physical and hydrodynamic characteristics of restored (restoration age: <1 y, 2 y, 4 y) and intact reference-condition intertidal oyster reefs in a microtidal estuary. This study was designed to investigate differences between restored and intact oyster reefs, as well describe any hydrodynamic changes that may be linked to restoration age. We observed no significant differences in above-reef hydrodynamics for the reference and restored reefs described in this study, with similar magnitudes for both mean flow (i.e. velocity attenuation) and turbulence ($\overline{w'^2}$, ϵ, P/ϵ, u_s^2/U_R^2) parameters. Minor differences in hydrodynamics on live reference and restored reefs were limited to channel-to-reef velocity attenuation and mixing near the bed, where turbulence characteristics were significantly more variable than those measured above the complex oyster canopy. By contrast, significant differences in flow and turbulence were observed between live (i.e. reference and restored) and degraded reefs, with order of magnitude increases in mixing within live oyster canopies and a near complete disconnect between channel and reef currents on the fringes of the degraded reef. Considering the previously degraded state of restored reefs, this study highlights a dramatic change in on-reef hydrodynamics facilitated through successful restoration practices. Although there was some variability in near-bed flow characteristics on live reefs, likely attributed to spatial canopy heterogeneity, we found no evidence to suggest that intact and restored reefs were functionally different in terms of hydrodynamic effects on the overlying flow. Results were used to conclude that restored reefs may reach hydrodynamic similarity with natural intact reefs within 1 year of restoration, assuming restoration strategies are successful and site conditions provide ample opportunity for oyster recruitment.

CRediT authorship contribution statement

David Cannon: Validation, Formal analysis, Visualization, Writing – original draft, Writing – review & editing. **Kelly M. Kibler:** Conceptualization, Investigation, Supervision, Writing – original draft, Writing – review & editing. **Vasileios Kitsikoudis:** Conceptualization, Investigation, Writing – review & editing. **Stephen C. Medeiros:** Conceptualization, Investigation, Writing – review & editing. **Linda J. Walters:** Conceptualization, Investigation, Writing – review & editing.

Declaration of Competing Interest

The authors declare that they have no known competing financial interests or personal relationships that could have appeared to influence the work reported in this paper.

Acknowledgments

This work was funded by the U.S. National Science Foundation (NSF grants #1617374 and 1944880), and the University of Central Florida, with in-kind support provided by the National Park Service. We are also grateful to David W. Spiering and Barbara Nogueira Tirado for their help in field measurements. The authors declare that there is no conflict of interest. The data presented in this manuscript are available through the National Centers for Environmental Information (Cannon et al., 2021).

References

ASTM, 2006. Standard Test Method for Sieve Analysis of Fine and Coarse Aggregates.
ASTM, 2013. Standard Test Method for Materials Finer than 75-um (No. 200) Sieve in Mineral Aggregates by Washing.

Barber, A., Walters, L., Birch, A., 2010. Potential for restoring biodiversity of macroflora and macrofauna on oyster reefs in Mosquito Lagoon. Florida Florida Sci. 73, 47–62.
Beck, M.W., Brumbaugh, R.D., Airoldi, L., et al., 2011. Oyster reefs at risk and recommendations for conservation, restoration, and management. Bioscience 61, 107–116. https://doi.org/10.1525/bio.2011.61.2.5.
Bricker, J.D., Monismith, S.G., 2007. Spectral wave–turbulence decomposition. J. Atmos. Ocean. Technol. 24, 1479–1487.
Cannon, D.J., Troy, C.D., 2018. Observations of turbulence and mean flow in the low-energy hypolimnetic boundary layer of a large lake. Limnol. Oceanogr. 63, 2762–2776. https://doi.org/10.1002/lno.11007.
Cannon, D., Kibler, K., Kitsikoudis, V., Medeiros, S., Walters, L., Spiering, D., Nogueira, B., 2021. Mean Flow and Turbulence Observations on Reference and Restored Oyster Reefs in Mosquito Lagoon - Florida from 2018-06-01 to 2018-11-15 (NCEI Accession 0225430). NOAA National Centers for Environmental Information. Dataset. https://doi.org/10.25921/f389-7q16.
Cannon, D., Kibler, K., Walters, L., Chambers, L., 2022. Hydrodynamic and biogeochemical evolution of a restored intertidal oyster (*Crassostrea virginica*) reef. Sci. Total Environ. 154879.
Chambers, L.G., Gaspar, S.A., Pilato, C.J., Steinmuller, H.E., McCarthy, K.J., Sacks, P.E., Walters, L.J., 2018. How well do restored intertidal oyster reefs support key biogeochemical properties in a coastal lagoon? Estuar. Coasts 41, 784–799. https://doi.org/10.1007/s12237-017-0311-5.
Coen, L.D., Luckenbach, M.W., 2000. Developing success criteria and goals for evaluating oyster reef restoration: Ecological function or resource exploitation? Ecol. Eng. 15, 323–343. https://doi.org/10.1016/S0925-8574(00)00084-7.
Coen, L.D., Luckenbach, M.W., Breitburg, D.L., 1999. The role of oyster reefs as essential fish habitat: a review of current knowledge and some new perspectives. Am. Fish. Soc. Symp. 438–454.
Colden, A.M., Fall, K.A., Cartwright, G.M., Friedrichs, C.T., 2016. Sediment suspension and depositionacross restored oyster reefs of varying orientation to flow: Implications for restoration. Estuar. Coasts 39, 1435–1448. https://doi.org/10.1007/s12237-016-0096-y.
Dame, R.F., Spurrier, J.D., Wolaver, T.G., 1989. Carbon, nitrogen, and phosphorous processing by an oyster reef. Mar. Ecol. Prog. Ser. 54, 249–256.
Davis, K.A., Pawlak, G., Monismith, S.G., 2021. Turbulence and coral reefs. Annu. Rev. Mar. Sci. 13 https://doi.org/10.1146/annurev-marine-042120-071823.
Dean, R.G., Dalrymple, R.A., 1991. Water Wave Mechanics for Engineers and Scientists, Advanced S. World Scientific Publishing Co.
Down, C., Withrow, R., 1978. Vegetation and Other Parameters in the Brevard County Bar-Build Estuaries.
Elliott, M., Burdon, D., Hemingway, K.L., Apitz, S.E., 2007. Estuarine, coastal and marine ecosystem restoration: confusing management and science - a revision of concepts. Estuar. Coast. Shelf Sci. 74, 349–366. https://doi.org/10.1016/j.ecss.2007.05.034.
Elliott, M., Mander, L., Mazik, K., Simenstad, C., Valesini, F., Whitfield, A., Wolanski, E., 2016. Ecoengineering with ecohydrology: successes and failures in estuarine restoration. Estuar. Coast. Shelf Sci. 176, 12–35. https://doi.org/10.1016/j.ecss.2016.04.003.
Finnigan, J., 2000. Turbulence in plant canopies. Annu. Rev. Fluid Mech. 32, 519–571. https://doi.org/10.1146/annurev.fluid.32.1.519.
Fodrie, F.J., Rodriguez, A.B., Gittman, R.K., Grabowski, J.H., Lindquist, N.L., Peterson, C. H., Piehler, M.F., Ridge, J.T., 2017. Oyster reefs as carbon sources and sinks. Proc. R. Soc. B Biol. Sci. 284, 20170891. https://doi.org/10.1098/rspb.2017.0891.
Garvis, S.K., Sacks, P.E., Walters, L.J., 2015. Formation, movement, and restoration of dead intertidal oyster reefs in Canaveral National Seashore and Mosquito Lagoon. Florida J. Shellfish Res. 34, 251–258. https://doi.org/10.2983/035.034.0206.
Gillies, C.L., Crawford, C., Hancock, B., 2017. Restoring Angasi oyster reefs: What is the endpoint ecosystem we are aiming for and how do we get there? Ecol. Manag. Restor. 18, 214–222.
Goring, D.G., Nikora, V.I., 2002. Despiking acoustic Doppler velocimeter data. J. Hydraul. Eng. 128, 117–126. https://doi.org/10.1061/(asce)0733-9429(2002)128:1(117).
Grabowski, J.H., Brumbaugh, R.D., Conrad, R.F., et al., 2012. Economics valuation of ecosystem services provided by oyster reefs. Bioscience 62, 900–909. https://doi.org/10.1525/bio.2012.62.10.10.
Grizzle, R.E., Adams, J.R., Walters, L., 2002. Historical changes in intertidal oyster (*crassostrea virginica*) reefs in a. J. Shellfish Res. 21, 749–756.
Gutiérrez, J.L., Jones, C.G., Strayer, D.L., Iribarne, O.O., 2003. Mollusks as Ecosystem Engineers: The Role of Shell Production in Aquatic Habitats. Oikos. John Wiley & Sons, Ltd, pp. 79–90.
Hansen, J.C.R., Reidenbach, M.A., 2017. Turbulent mixing and fluid transport within Florida Bay seagrass meadows. Adv. Water Resour. 108, 205–215. https://doi.org/10.1016/j.advwatres.2017.08.001.
Hubbard, A.B., Reidenbach, M.A., 2015. Effects of larval swimming behavior on the dispersal and settlement of the eastern oyster *Crassostrea virginica*. Ma. Ecol. Prog. Ser. (535), 161–176.
Kaplan, D.A., Olabarrieta, M., Frederick, P., Valle-Levinson, A., 2016. Freshwater detention by oyster reefs: quantifying a keystone ecosystem service. PLoS One 11 (12), e0167694.
Kastner-Klein, P., Rotach, M.W., 2004. Mean flow and turbulence characteristics in an urban roughness sublayer. Boundary-Layer Meteorol. 111, 55–84. https://doi.org/10.1023/B:BOUN.0000010994.32240.b1.
Kibler, K.M., Kitsikoudis, V., Donnelly, M., Spiering, D., Walters, L., 2019. Flow-vegetation interaction in a living shoreline restoration and potential effect to mangrove recruitment. Sustainability 11 (11).
Kitsikoudis, V., Kibler, K.M., Walters, L.J., 2020. In-situ measurements of turbulent flow over intertidal natural and degraded oyster reefs in an estuarine lagoon. Ecol. Eng. 143, 105688 https://doi.org/10.1016/j.ecoleng.2019.105688.
La Peyre, M.K., Humphries, A.T., Casas, S.M., La Peyre, J.F., 2014. Temporal variation in development of ecosystem services from oyster reef restoration. Ecol. Eng. 63, 34–44. https://doi.org/10.1016/j.ecoleng.2013.12.001.
Lenihan, H.S., 1999. Physical-biological coupling on oyster reefs: how habitat structure influences individual performance. Ecol. Monogr. 69, 251–275. https://doi.org/10.1890/0012-9615(1999)069[0251:PBCOOR]2.0.CO;2.
Locher, B., Hurst, N.R., Walters, L.J., Chambers, L.G., 2020. Juvenile oyster (*Crassostrea virginica*) biodeposits contribute to a repid rise in sediment nutrients on restored intertidal oyster reefs (Mosquito Lagoon, FL, USA). Estuar. Coasts 1–17. https://doi.org/10.1007/s12237-020-00874-2.
McClenachan, G.M., Donnelly, M.J., Shaffer, M.N., Sacks, P.E., Walters, L.J., 2020. Does size matter? Quantifying the cumulative impact of small-scale living shoreline and oyster reef restoration projects on shoreline erosion. Restor. Ecol. 28, 1365–1371. https://doi.org/10.1111/rec.13235.
McFarland, K., Hare, M.P., 2018. Restoring oysters to urban estuaries: Redefining habitat quality for eastern oyster performance near New York City J.A. Fernández Robledo. PLoS One 13, e0207368. https://doi.org/10.1371/journal.pone.0207368.
Mehta, A.J., Brooks, H.K., 1973. Mosquito Lagoon barrier beach study. Shore Beach 41, 27–34.
Meyer, D.L., Townsend, E.C., Thayer, G.W., 1997. Stabilization and erosion control value of oyster cultch for intertidal marsh. Restor. Ecol. 5, 93–99. https://doi.org/10.1046/j.1526-100X.1997.09710.x.
Monismith, S.G., 2007. Hydrodynamics of coral reefs. Annu. Rev. Fluid Mech. 39, 37–55.
Nepf, H.M., 2012. Flow and transport in regions with aquatic vegetation. Annu. Rev. Fluid Mech. 44, 123–142. https://doi.org/10.1146/annurev-fluid-120710-101048.
Ogburn, D.M., White, I., McPhee, D.P., 2007. The disappearance of oyster reefs from eastern Australian estuaries—impact of colonial settlement or mudworm invasion? Coast. Manag. 35 (2–3), 271–287.
Peterson, C., Grabowski, J., Powers, S., 2003. Estimated enhancement of fish production resulting from restoring oyster reef habitat: quantitative valuation. Mar. Ecol. Prog. Ser. 264, 249–264. https://doi.org/10.3354/meps264249.
Porter, E., Cornwell, J., Sanford, L., 2004. Effect of oysters *Crassostrea virginica* and bottom shear velocity on benthic-pelagic coupling and estuarine water quality. Mar. Ecol. Prog. Ser. 271, 61–75. https://doi.org/10.3354/meps271061.
Reidenbach, M.A., Monismith, S.G., Koseff, J.R., Yahel, G., Genin, A., 2006. Boundary layer turbulence and flow structure over a fringing coral reef. Limnol. Oceanogr. 51, 1956–1968. https://doi.org/10.4319/lo.2006.51.5.1956.
Reidenbach, M.A., Koseff, J.R., Monismith, S.G., 2007. Laboratory experiments of fine-scale mixing and mass transport within a coral canopy. Phys. Fluids 19, 075107. https://doi.org/10.1063/1.2752189.
Reidenbach, M.A., Berg, P., Hume, A., Hansen, J.C.R., Whitman, E.R., 2013. Hydrodynamics of intertidal oyster reefs: the influence of boundary layer flow processes on sediment and oxygen exchange. Limnol. Oceanogr. Fluids Environ. 3, 225–239. https://doi.org/10.1215/21573689-2395266.
Ridge, J.T., Rodriguez, A.B., Joel Fodrie, F., Lindquist, N.L., Brodeur, M.C., Coleman, S. E., Grabowski, J.H., Theuerkauf, E.J., 2015. Maximizing oyster-reef growth supports green infrastructure with accelerating sea-level rise. Sci. Rep. 5, 14785. https://doi.org/10.1038/srep14785.
Rodriguez, A.B., Fodrie, F.J., Ridge, J.T., et al., 2014. Oyster reefs can outpace sea-level rise. Nat. Clim. Chang. 4, 493–497.
Scannell, B.D., Rippeth, T.P., Simpson, J.H., Polton, J.A., Hopkins, J.E., 2017. Correcting surface wave bias in structure function estimates of turbulent kinetic energy dissipation rate. J. Atmos. Ocean. Technol. 34, 2257–2273. https://doi.org/10.1175/JTECH-D-17-0059.1.
Schulte, D.M., Burke, R.P., Lipcius, R.N., 2009. Unprecedented restoration of a native oyster metapopulation. Science 325 (5944), 1124–1128.
Solomon, J.A., Donnelly, M.J., Walterst, L.J., 2014. Effects of sea level rise on the intertidal oyster *Crassostrea virginica* by field experiments. J. Coast. Res. 68, 57–64. https://doi.org/10.2112/si68-008.1.
Stiner, J.L., Walters, L.J., 2008. Effects of recreational boating on oyster reef architecture and species interactions. Florida Sci. 71, 31–44.
Styles, R., 2015. Flow and turbulence over an oyster reef. J. Coast. Res. 31, 978–985. https://doi.org/10.2112/JCOASTRES-D-14-00115.1.
Thomas, R.E., Schindfessel, L., McLelland, S.J., Creëlle, S., De Mulder, T., 2017. Bias in mean velocities and noise in variances and covariances measured using a multistatic acoustic profiler: the Nortek Vectrino Profiler. Meas. Sci. Technol. 28, 075302 https://doi.org/10.1088/1361-6501/aa7273.
Trowbridge, J., Elgar, S., 2001. Turbulence measurements in the surf zone. J. Phys. Oceanogr. 31 (8), 2403–2417.
Veenstra, J., Southwell, M., Dix, N., Marcum, P., Jackson, J., Burns, C., Kemper, A., 2021. High carbon accumulation rates in sediment adjacent to constructed oyster reefs, Northeast Florida, USA. J. Coast. Conserv. 25 (4), 1–11.
Wahl, T.L., 2003. Discussion of "Despiking acoustic doppler velocimeter data" by Derek G. Goring and Vladimir I. Nikora J. Hydraul. Eng. 129, 484–487.
Walles, B., Troost, K., van den Ende, D., Nieuwhof, S., Smaal, A.C., Ysebaert, T., 2016. From artificial structures to self-sustaining oyster reefs. J. Sea Res. 108, 1–9.
Walters, L.J., Sacks, P.E., Bobo, M.Y., Richardson, D.L., Coen, L.D., 2007. Impact of hurricanes and boat wakes on intertidal oyster reefs in the Indian River Lagoon: reef profiles and disease prevalence. Florida Sci. 70, 506–521.
White, S.A., Stephen, A., Jeong, I., Hess, K.W., Wang, J., Myers, E.P., 2016. An assessment of the revised VDatum for eastern Florida, Georgia, South Carolina, and North Carolina C.S.D.L. (U.S.) [ed.]. https://doi.org/10.7289/V5/TM-NOS-CS-38.

Whitman, E., Reidenbach, M., 2012. Benthic flow environments affect recruitment of *Crassostrea virginica* larvae to an intertidal oyster reef. Mar. Ecol. Prog. Ser. 463, 177–191. https://doi.org/10.3354/meps09882.

Wilberg, M., Livings, M., Barkman, J., Morris, B., Robinson, J., 2011. Overfishing, disease, habitat loss, and potential extirpation of oysters in upper Chesapeake Bay. Mar. Ecol. Prog. Ser. 436, 131–144. https://doi.org/10.3354/meps09161.

Wiles, P.J., Rippeth, T.P., Simpson, J.H., Hendricks, P.J., 2006. A novel technique for measuring the rate of turbulent dissipation in the marine environment. Geophys. Res. Lett. 33, L21608. https://doi.org/10.1029/2006GL027050.

Wüest, A., Lorke, A., 2003. Small-Scale Hydrodynamics in Lakes. Annu. Rev. Fluid Mech. 35, 373–412. https://doi.org/10.1146/annurev.fluid.35.101101.161220.